Membrane-dependent modulation of the mTOR activator Rheb: NMR observations of a GTPase tethered to a lipid-bilayer nanodisc

Mohammad T. Mazhab-Jafari,[†] Christopher B. Marshall,[†] Peter B. Stathopulos,[†] Yoshihiro Kobashigawa,[‡] Vuk Stambolic,[†] Lewis E. Kay,[‖,⊥] Fuyuhiko Inagaki,[‡] and Mitsuhiko Ikura[†]*

†Department of Medical Biophysics, Campbell Family Cancer Research Institute, Ontario Cancer Institute, Princess Margaret Cancer Center, University Health Network, University of Toronto, Toronto, Ontario M5G 2M9, Canada. ‡Faculty of Advanced Life Science, Hokkaido University, Sapporo 001-0021, Japan ‖Departments of Molecular Genetics, Biochemistry, and Chemistry, University of Toronto, Toronto,ON, Canada M5S 1A8. ⊥Program in Molecular Structure and Function, Hospital for Sick Children, Toronto,ON, Canada M5G 1X8.

Experimental procedures:

Protein preparations: *Mus musculus* Rheb (residues 1-181) was prepared according to previous protocols[1]. In brief, the protein was expressed in *Escherichia coli* (BL21) using a pGEX2T vector and grown in minimal media supplemented with $^{15}NH_4Cl$ and induced at 15^{o}C with 0.25 mM IPTG. The protein was initially purified using glutathione Sepharose, cleaved from the GST tag by thrombin, with subsequent purification using Superdex 75 size exclusion chromatography in buffer A (20mM Tris pH 7.4, 100mM NaCl, 5mM $MgCl_2$, 1mM TCEP). Rheb typically yields ~20 mg/L of culture, and like other members of the small GTPase superfamily, it co-purified with endogenous guanine nucleotide. Membrane scaffold protein 1D1 (MSP1D1)[2] was prepared as described previously[3], with the following modifications. The protein was expressed in *Escherichia coli* (BL21) with pGBHPS–MSP in 2× TY media using a LEX^{TM} bioreactor system at 37 $^{\circ}$C with 1 mM IPTG for 1 h followed by further 2.5h incubation at 28 $^{\circ}$C. MSP was purified using His-tagged affinity purification followed by HRV3C protease-mediated His-tag cleavage and subsequent size exclusion chromatography using Superdex 75, with a typical yield of 40 mg/L of culture.

Preparation of Rheb-nanodisc complex: All lipids were purchased from Avanti Polar Lipids, Inc. Nanodiscs were prepared according to previous protocols[3] with the following modifications. 1,2-dioleoyl-*sn*-glycero-3-phosphocholine (DOPC) and the thiol-reactive lipid 1,2-dioleoyl-*sn*-glycero-3-phosphoethanolamine-N-[4-(p-maleimidomethyl)cyclohexane-carboxamide] (PE-MCC), were mixed with a molar ratio of 20:1 in a chloroform-ethyl alcohol solution. For PRE experiments, 1,2-distearoyl-

sn-glycero-3-phosphoethanolamine-N-diethylenetriaminepentaacetic acid (gadolinium salt) (PE-DTPA (Gd^{3+})) was added to the lipids at a molar ratio of 20 DOPC : 1 PE-MCC : 1 PE-DTPA (Gd^{3+}). The organic solvents were then removed using gentle nitrogen flow followed by vacuum, and the dried lipid film was solubilized in aqueous buffer containing detergent (20mM Tris pH 7.4, 100mM NaCl, and 100mM sodium cholate). This mixture was subjected to three freeze/thaw cycles, vortexed until clarified, then MSP1D1 was added at a 1:40 molar ratio relative to the lipids [3]. Following 1 h incubation with mild rotation at 20 °C, sodium cholate was removed from the MSP-lipid mixture with Bio-Beads SM-2 Adsorbents (Bio-RAD) using a batch method with 2h incubation at room temperature with mild rotation. The nanodisc particles were then purified via size exclusion chromatography using a 26-60 Superdex 200 column equilibrated with buffer A without TCEP. The particle size were analyzed with dynamic light scattering (DLS) and corresponded with a 10nm diameter particle (data not shown). Rheb 1-181 was passed through a 10-30 Superdex S75 column equilibrated with buffer A without TCEP at 4^{o}C to remove reducing agent, and was immediately added to the nanodisc preparation at a 2:1 molar ratio (one Rheb molecule for each face of the nanodisc). The conjugation reaction was allowed to proceed for 16h at room temperature, then the mixture was passed through a Superdex 200 column equilibrated with buffer A to separate free Rheb from nanodisc-bound Rheb. The concentration of the nanodisc-Rheb complex was estimated by SDS-PAGE and size exclusion chromatography analysis.

NMR- measurements: NMR measurements were carried out on either a Bruker AVANCE II 800 MHz spectrometer equipped with a 5 mm TCI CryoProbe^{TM} or a 600 MHz spectrometer equipped with TCI 1.7 mm MicroCryoProbe^{TM}. The spectra were acquired at a temperature of 20^{o} C using samples containing 0.3mM free Rheb or 0.6mM nanodisc-conjugated Rheb. To monitor GTPase reactions in real-time, sensitivity enhanced ^{1}H-^{15}N heteronuclear single quantum coherence (HSQC) spectra with 8 scans (18 min) each were collected in succession as previously described[1]. For analysis of chemical shift perturbation and PRE experiments, 32 scans (72min) were used. No GDP resonances were observable above the spectral noise in the 32-scan $^{15}N^{1}H$-HSQC of a GTP-loaded Rheb sample indicating that any hydrolysis occurring during data collection was not appreciable. For PRE measurements, the resonance intensities of ^{15}N Rheb on PE-DTPA (Gd^{3+})-containing nanodiscs were compared to those of a control sample prepared without PE-DTPA (Gd^{3+}). No PE-DTPA-chelated diamagnetic ion is available to serve as a control, however the absence of any detectable chemical shift differences in the Rheb spectrum in the absence or presence of 5% (mole fraction to total lipid) PE-DTPA suggests that PE-DTPA-free nanodiscs provide an appropriate control to monitor the PRE-effect. The cross-peak intensities were

measured using Sparky[4] and Gaussian line fitting. The difference in concentration between the PRE and the control samples was less than 10%, as judged by the size exclusion chromatogram and SDS-PAGE. This difference in concentration was corrected by normalization of the calculated intensity ratios against the highest observed I*/Io (where I* is the resonance intensities of Rheb conjugated to nanodiscs incorporating 5% Gd3+-conjugated PE-DTPA, and Io is that in the paramagnetic ion-free nanodiscs) for each GDP and GTP plot. Residues in the β1-α1 and β4-α3 loops, which are in close proximity to each other and close to the nucleotide binding pocket, exhibited the least PRE and were therefore used as an internal standard for the normalization, for GDP and GTP, respectively. For comparing GDP and GTP plots, this normalization process was evaluated using the PRE-effect on Cys181, which is covalently linked to the surface of the membrane, and thus would be expected to exhibit similar PRE, independent of the bound nucleotide. Indeed, Cys181 was similarly broadened in GDP- and GTP-bound samples (96.0% and 95.5 %, respectively). For relaxation experiments, the ^{15}N longitudinal and transverse relaxation rates R_1 and R_2, as well as the $\{^1H\}$ ^{15}N steady-state NOEs were measured using 0.3mM samples of free ^{15}N Rheb-GDP and -GMPPNP (Δ182-184) and samples of 0.6mM ^{15}N Rheb-GDP and -GMPPNP (Δ182-184) conjugated to 0.3 mM nanodiscs. Rheb was pre-loaded with GMPPNP in the presence of EDTA- and alkaline phosphatase, as described previously[1], prior to nanodisc conjugation. Backbone relaxation measurements were performed at 800MHz. Recycle delays of 3.0, 2.5, and 4.0 sec were used for ^{15}N R1, ^{15}N R2, and $\{^1H\}$ ^{15}N steady state NOE acquisitions, respectively. The relaxation delays (^{15}N R1 experiments:10, 180, 900, 265, 700, 1400, 350, 1100, 265, and 10 ms, and R2 experiments: 15.84, 63.36, 31.68, 95.04, 47.52, 84.20, 110.9, 63.36, and 15.84 ms) were varied in non-sequential order (as listed) to avoid systematic stability-related fluctuations in peak intensities, and duplicate delay times were used to ensure sample stability and estimate errors in fitting curves. Sample stability was monitored by intermediate HSQCs between T1, T2, and $\{^1H\}$ ^{15}N steady state NOE measurements. ^{15}N R1 and ^{15}N R2 experiments were run with 16 scans, and 64 scans were acquired for $\{^1H\}$ ^{15}N steady state NOEs. The overall rotational correlation time (τ_M) was calculated as previously detailed[5]. In brief, the values of the spectral density functions $J(0.870\omega_H)$, $J(\omega_N)$, and $J(0)$ were determined from the mean of R1, R2 and $\{^1H\}$ ^{15}N steady state NOEs using equations 12-14 from Farrow *et al*[5], in which no prior assumption is made on the structure of the molecule. Of the values of ^{15}N R1, ^{15}N R2, and $\{^1H\}$ ^{15}N steady state NOEs determined for each peak, the top and bottom 10% were excluded from the calculation. The value of the spectral density function at zero frequency was then used to derive the (τ_M) using the form of the spectral density function derived from model-free

formalism (equation 4 in Farrow *et al*[5]) assuming limited (large order parameter, S^2) and fast (<10ps) internal motions. The variations in the trimmed means of R1, R2, and $\{^1H\}$ ^{15}N steady state NOEs were used in error calculations.

Real-time NMR-based GTPase assay: Assays of Rheb GTPase function were carried out as described previously[1]. In brief, nucleotide exchange reactions were initiated by adding a 5-fold molar excess of GTP to a GDP-loaded ^{15}N Rheb sample, and monitored via successive 8-scan ^{15}N ^1H HSQC spectra (18min). TSC2GAP-catalyzed reactions were initiated by adding extracts of HEK-293 cells over-expressing full length TSC1 and TSC2 as described previously[6]. The reactions were initiated with cell extracts prepared by mechanical lysis. Expression of TSC2 in these lysates was confirmed by Western blots (data not shown).

Molecular docking simulation: All docking simulations were performed with gpc supercomputer at the SciNet[7] HPC Consortium using High Ambiguity Driven biomolecular DOCKing (HADDOCK) sofware version 2.1[8, 9]. The structures of GDP- and GTP-bound of *Mus musculus* Rheb (residues 1-181) were annealed in CNS using the RECOORD scripts[10] from starting extended polypeptide chains using distance, hydrogen bond, and torsion angle restraints derived from the crystal structures of human Rheb GDP and GTP (1XTQ and 1XTS, respectively)[11], which share 99% sequence identity. No restraints were given for 1-MP-2 and 172-DGAASQGKSSC-181 residues during the annealing protocol so that these Rheb termini sampled a large conformational variability in the final ensemble of structures consistent with our $\{^1H\}$ - ^{15}N steady state NOEs. The G-domains (residues 4-171) of the 20 lowest energy annealed structures were all within 0.1 Å backbone rmsd of the template crystal structures. Each of the 20 lowest-energy structures for Rheb-GDP and Rheb-GTP were used as starting models in HADDOCK. The coordinate file for a nanodisc model[12] contained 80 1-palmitoyl-2-oleoyl-*sn*-glycero-3-phosphocholine (POPC) lipids per leaflet (i.e. 160 total), encompassed by 2 MSP polypeptide chains. The acyl chain of POPC is shorter than that of DOPC by two C atoms, but they share the same headgroup, thus their bilayer surfaces would be virtually identical.

HADDOCK ambiguous restraints were generated using the PRE-measurements on nanodisc-tethered Rheb. Because the lateral diffusion rate of DOPC at room temperature (~8.2×10^3 nm^2/ms)[13] is high relative to T2 relaxation times of Rheb on nanodiscs (~30 ms), an assumption was made that the PRE tag uniformly sampled all positions on the nanodisc surface (78 nm^2) during the time course of the measurement. Thus, ambiguous restraints were generated between PRE-affected residues on Rheb (e.g. Gly51) and "any" lipid headgroup atom on the nanodisc surface (*e.g.* G51 to lipid-$1_{[N1 \text{ or } C13 \text{ or } C14 \text{ or } C15 \text{ or}}$

P1 or O11 …] or lipid-2[N1 or C13 or C14 or C15 or P1 or O11 …] or …). Residues in Rheb with peaks displaying >80% broadening were defined in HADDOCK as 'active' residues and those broadened between 50% and 80% were defined as passive residues. For the Rheb-GDP-nanodisc complex the active residues were 1, 3, 6, 51, 77, 110, 172, 173, 174, 175, 176, 177, 178, 179, 180, 181, and the passive residues were 5, 7, 47, 48, 49, 53, 55, 74, 75, 76, 78, 106, 107, 108, 132, 114, 141, 143, 144, 145, 154, 162, 164, 169, 171. For the Rheb-GTP-nanodisc the active residues were 1, 3, 6, 48, 51, 110, 172, 173, 174, 175, 176, 177, 178, 179, 180, 181, and the passive residues were 5, 7, 49, 53, 54, 108, 109, 114, 115, 132, 140, 141, 143, 144, 145, 154, 162, 166, 171. The ambiguous restraints were assigned a distance range of 2-10 Å from any atom of any lipid headgroup. Although Gd^{3+} is known to affect nuclear spin magnetization within a 20 Å radius[14], the upper limit of 10 Å was selected because i) each lipid head group on the membrane surface is only partially occupied by Gd^{3+}-conjugated lipid which comprises 5% of the total lipids, and ii) active residues were stringently defined (i.e. >80% broadening) in HADDOCK. An upper limit of 2 Å was selected for Cys181 of Rheb, since it was covalently linked to the membrane surface. The CNS topology and the parameter files for the nucleotides and POPC lipids were initially generated using the HIC-UP server[15] and modified according to the data listed for these small molecules in the Automated Topology Builder (ATB) and Repository[16]. The docking protocol consisted of a 3000 rigid-body docking stage, where the top 300 ranked structures based on the HADDOCK score were refined using semi-flexible simulated annealing. The docking protocol was executed using the default HADDOCK script parameters except an additional Powell energy minimization step was performed on the lipid headgroups prior to the semi-flexible refinement stage.

Pairwise backbone rmsd values were tabulated for the Rheb G-domain (residues 4-171) after alignment of the nanodiscs on the same plane and a translational and 360° rotational (in 5° increments) rmsd minimization search confined only to movements within the 2D plane of the membrane surface in order to structurally align the Rheb molecules relative to the large lateral dimension of the nanodisc. The Rheb-nanodisc position in each solution was kept constant during pairwise rmsd calculation. Cluster analysis was then performed on the pairwise rmsd values using a previously described algorithm[17], setting an rmsd cutoff of 8 Å and cluster size cutoff of 30 structures. The HADDOCK scores of all 300 structures were plotted against rmsd relative to the global mean structure, defined as the solution with the lowest average pairwise rmsd to all other 299 solutions (Fig S4). To estimate the orientation angles, a vector was defined along the α6-helix of Rheb's G-domain, and the minimum angle between the long axis of α6 and the nanodisc membrane surface was measured for each complex. All structural

manipulations and measurements in three-dimensional space were performed using Crystallography & NMR System (CNS)[18]. The top 20% HADDOCK-scored complex structures of each cluster, as well as the cluster center models for each nucleotide-bound state, have been deposited in PDB/BMRB (PDB codes 2M4A (GDP) and 2M4B (GTP); BMRB accession numbers 18996 (GDP) and 18997 (GTP)).

Supplementary Figure Legends:

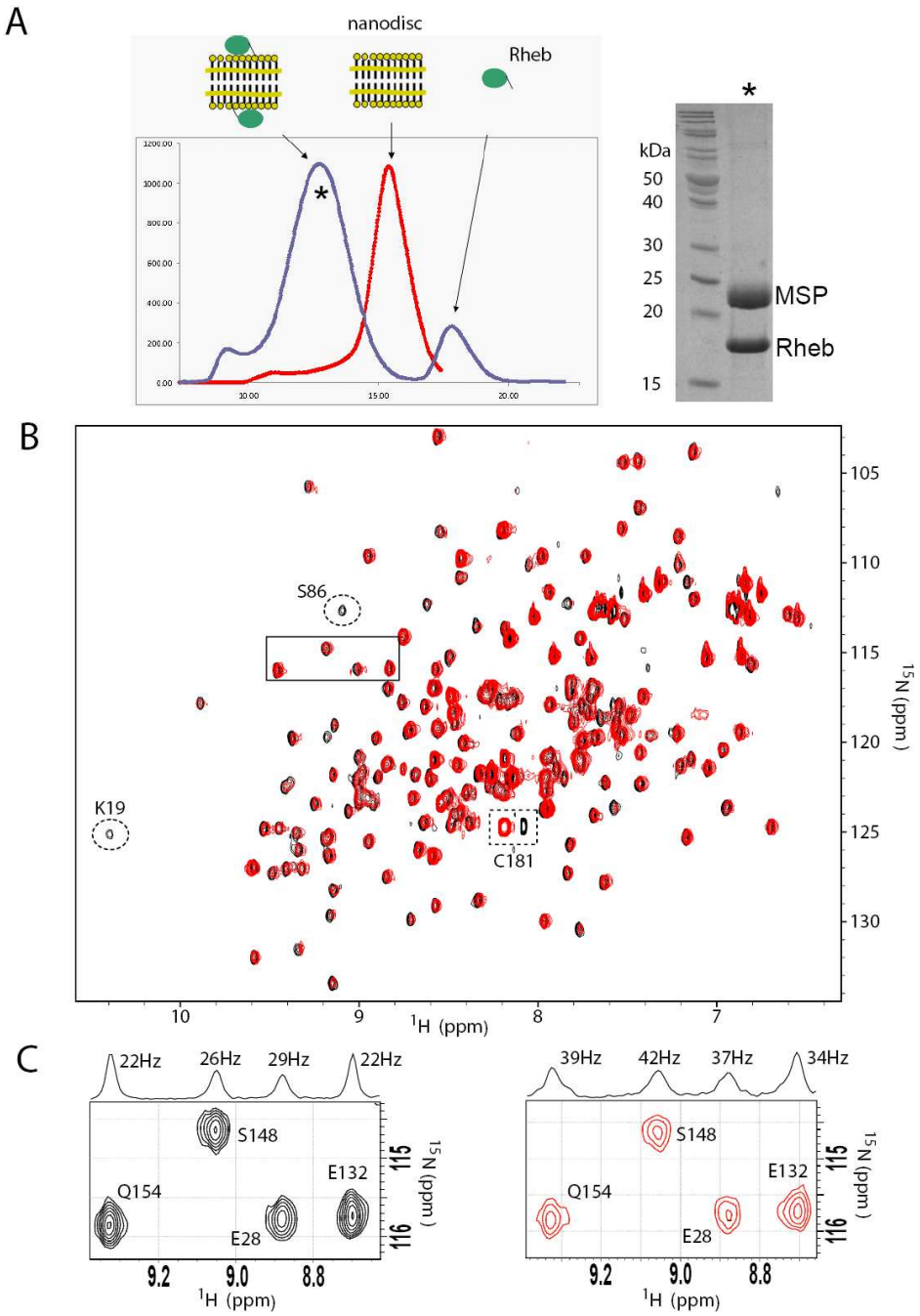

Figure S1: Preparation of Rheb-nanodisc complex. (A) Superdex S200 chromatograms of nanodiscs before and after conjugation with Rheb. SDS-PAGE analysis of the fraction containing Rheb-tethered nanodiscs (*) indicates a ~1:1 ratio of Rheb to MSP. (B) $^{15}N^{1}H$-HSQC spectra of 0.3 mM free (black) and 0.6 mM nanodisc-conjugated (red) Rheb-GDP. The only peak (Cys181) exhibiting appreciable chemical shift change upon membrane conjugation is shown with a dashed rectangle. Resonances with low S/N in free Rheb that are broadened beyond detection upon membrane conjugation are shown with dashed circles. C) Linewidths of free (black) versus nanodisc-conjugated (red) Rheb. The region illustrated is indicated by a solid rectangle in B and is shown at the same contour level in C.

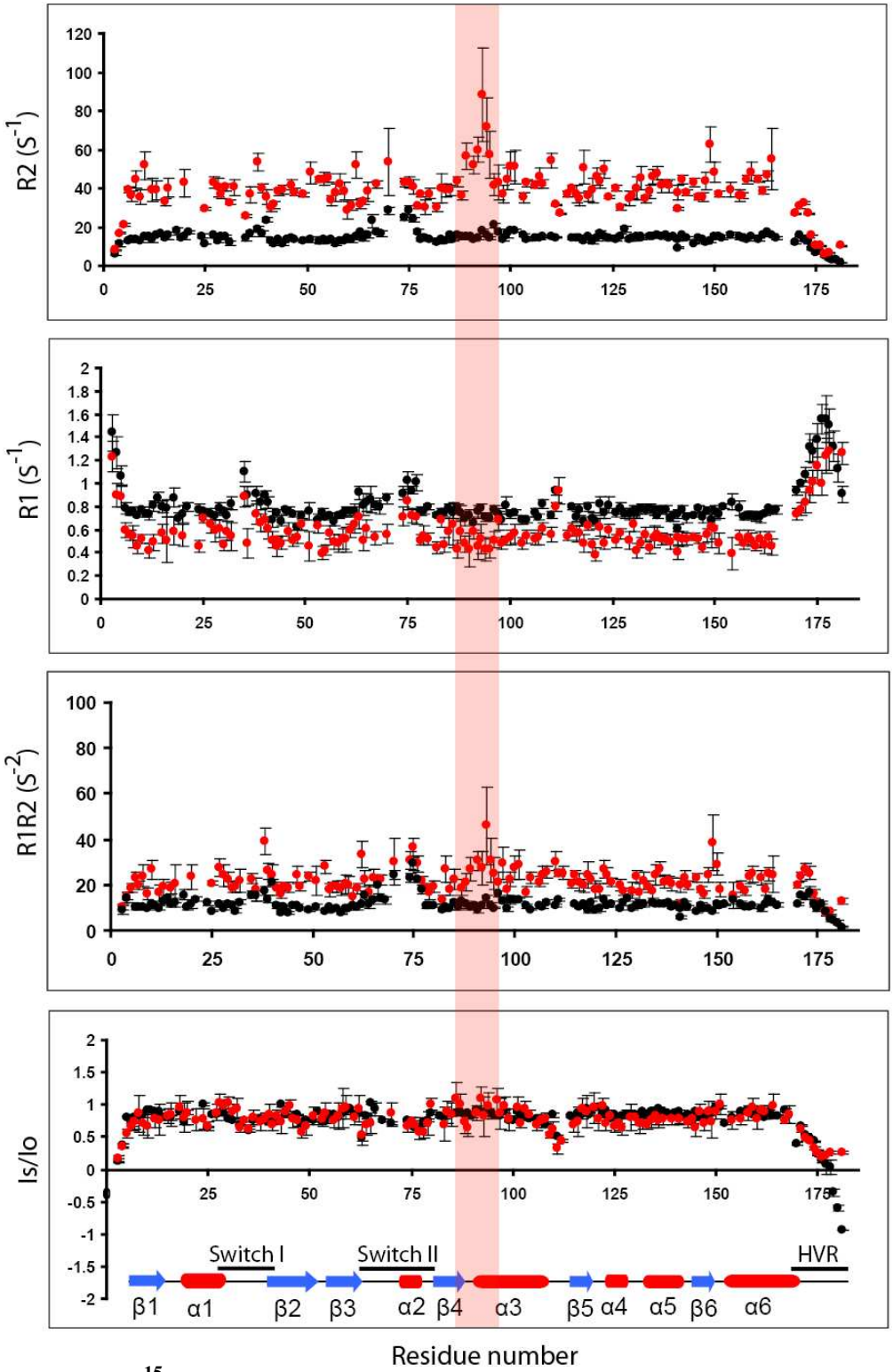

Figure S2: Backbone ^{15}N relaxation data for Rheb-GDP 1-181 in free (black) and nanodisc-bound (red) states. From top to bottom, transverse (^{15}N R2) relaxations, longitudinal (^{15}N R1) relaxations, R1×R2 products, and the {^{1}H} ^{15}N steady state NOE ($I_{saturated}/I_{unsaturated}$), each plotted against the residue number. The α3-helix, which exhibits increased R2 and R1R2, is highlighted in red.

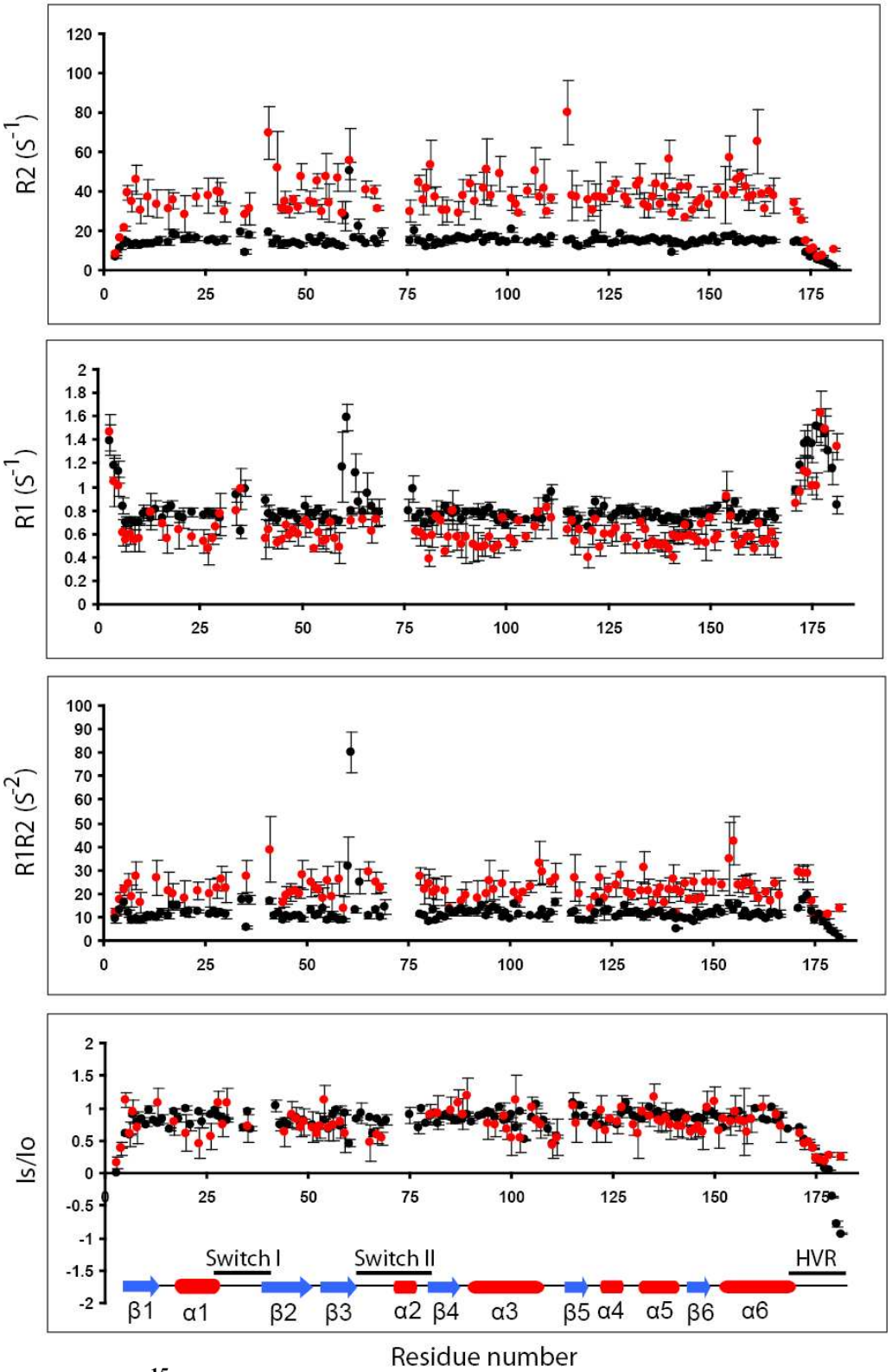

Figure S3: Backbone ^{15}N relaxation data for Rheb-GMPPNP 1-181 in free (black) and nanodisc-bound (red) states. From top to bottom, transverse relaxations (R2), longitudinal (^{15}N R1) relaxations, R1×R2 products, and the {^{1}H} ^{15}N steady state NOE, each plotted against the residue number.

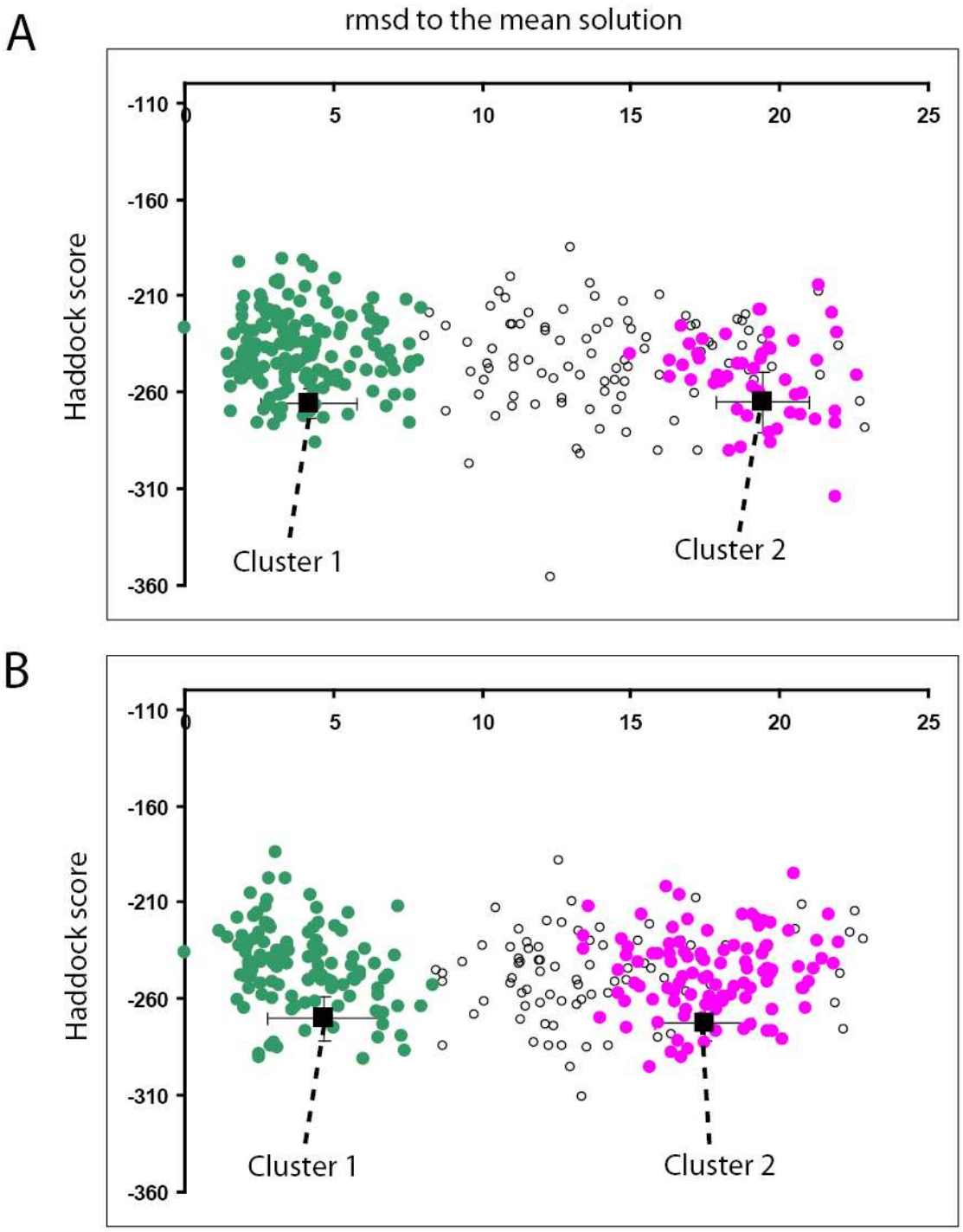

Figure S4: Cluster analysis of final HADDOCK solutions. The final 300 complex structures, represented with empty black circles are displayed in a plot of HADDOCK score versus rmsd to the global mean structure (defined as the structure with lowest rmsd to all other 299 structures) for (A) Rheb-GDP-nanodisc and (B) Rheb-GTP-nanodisc simulations. Complex structures belonging to cluster 1 (semi-perpendicular orientation, as described in the main text) and cluster 2 (semi-parallel orientation) are highlighted with green and magenta, respectively. The average HADDOCK score and rmsd (± standard deviation) of the 30 complex structures with lowest HADDOCK scores in each cluster is plotted as a filled black rectangle.

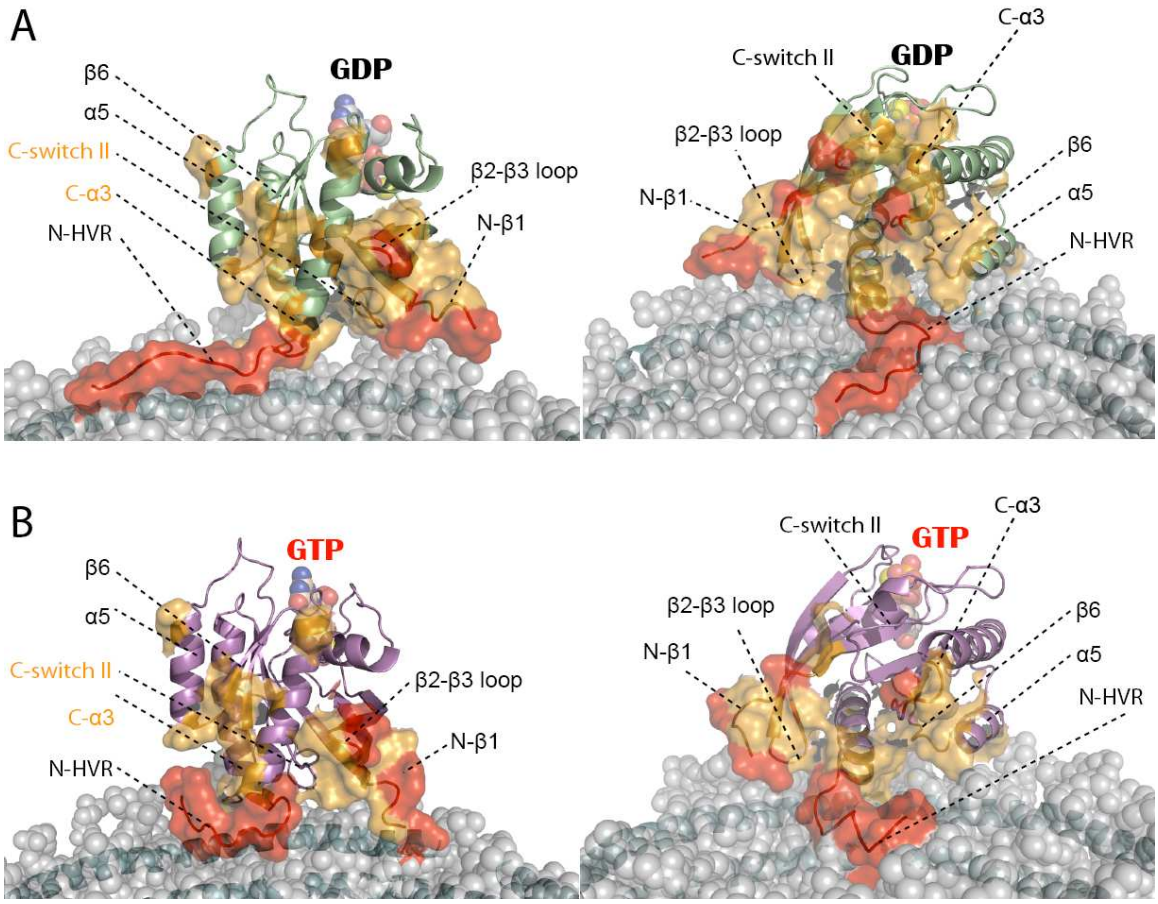

Figure S5: Residues affected by PRE localized on the HADDOCK models. The cluster center models of Rheb-nanodisc complexes are shown as follows; (A) Rheb-GDP in orientation 1 (left) and 2 (right), (B) Rheb-GTP in orientation 1 (left) and 2 (right). Residues exhibiting I*/Io < 0.5 and < 0.2 as described in Figure 2A are colored orange and red, respectively for Rheb-GDP and -GTP. The orange text indicates that the highlighted region is at the back of the page.

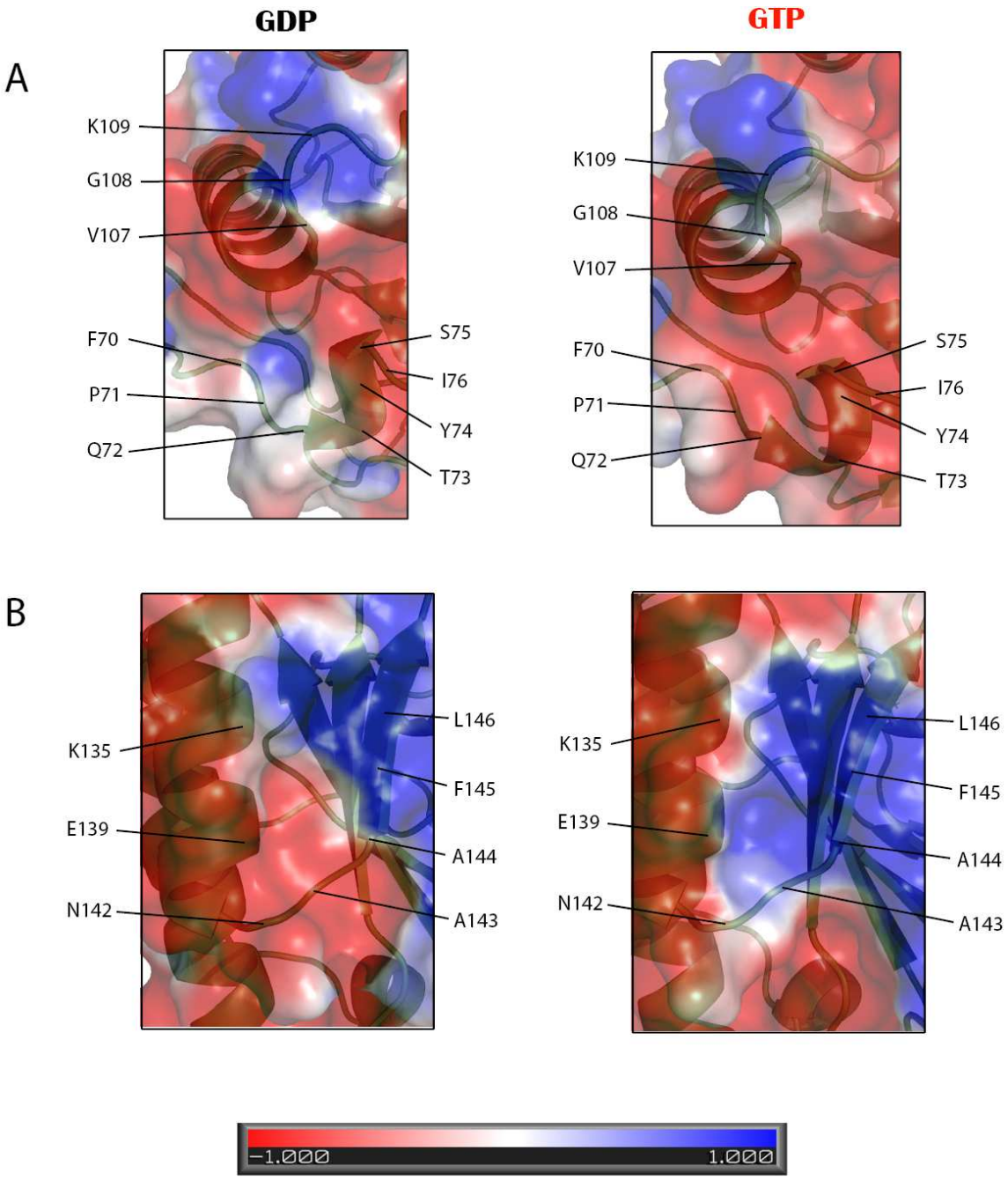

Figure S6: Subtle changes in surface electrostatics upon nucleotide exchange. The lowest energy annealed structures of Rheb (residues 1-181) before docking simulations. Rheb-GDP and -GTP are shown on the left and right of each panel, respectively. Panels A and B represent the electrostatic surfaces of the switch II-α3 (interface 1) and α5-β6 (interface 2) motifs, respectively. In the electrostatic surface, red, blue and gray represent negative, positive and neutral (hydrophobic) surfaces. The surface electrostatics were generated using the macromolecular electrostatics calculation program Adaptive Poisson-Boltzmann Solver (APBS)[19], and visualized via PyMOL.

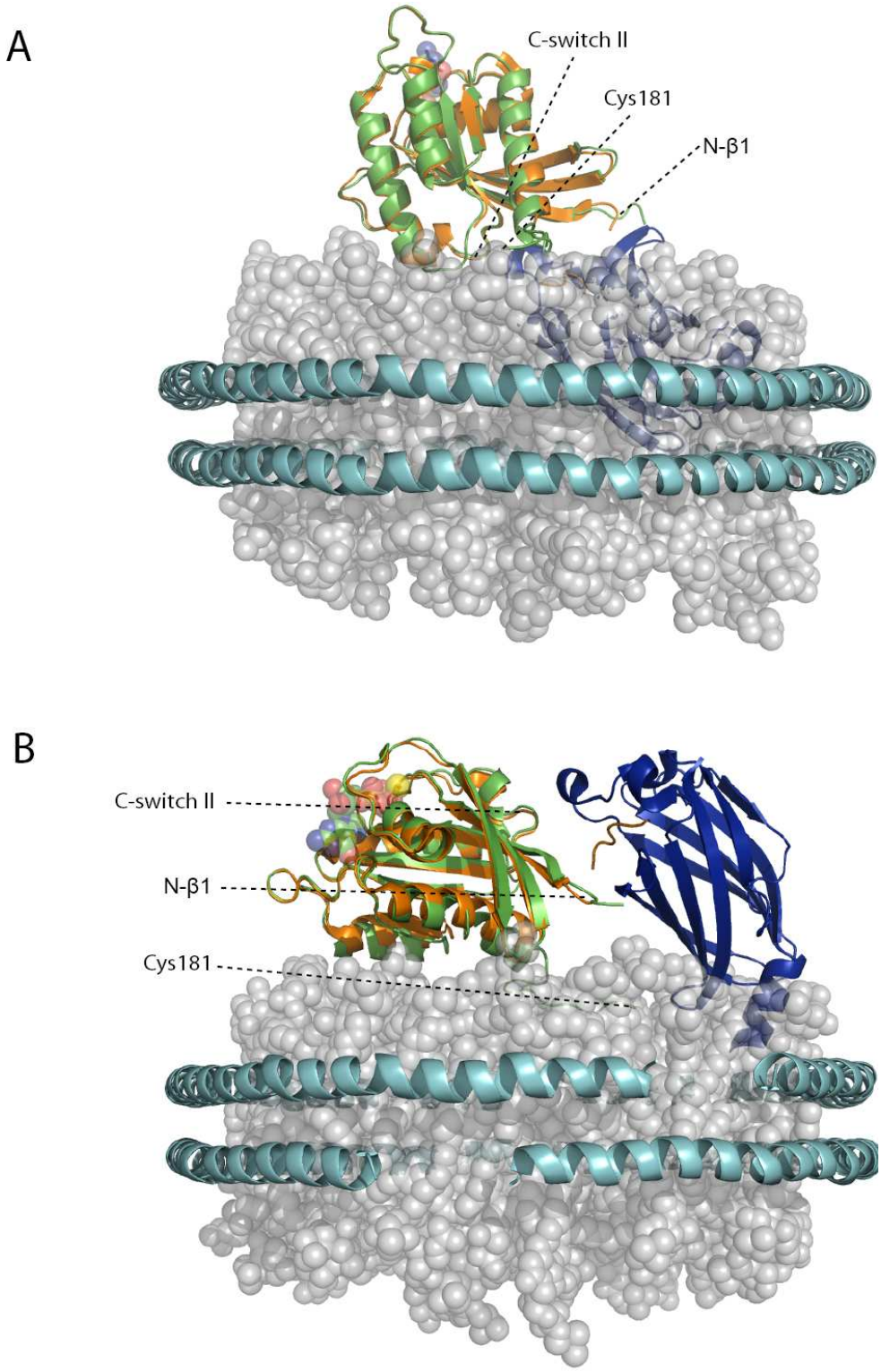

Figure S7: Formation of a Rheb-PDEδ complex is compatible with Rheb-nanodisc model 2, but not model 1. Cluster center structures for models 1 and 2 from Rheb-GDP docking simulations are shown in green in A and B, respectively. The Rheb and PDEδ components of the Rheb-PDEδ complex (PDB: 3T5G) are shown in orange and blue, respectively, and were aligned with the G-domain of Rheb (residues 4-171). The nucleotide, Mg^{2+} ion, and all atoms of POPC are represented as spheres.

References:

1. Marshall, C. B.; Ho, J.; Buerger, C.; Plevin, M. J.; Li, G. Y.; Li, Z.; Ikura, M.; Stambolic, V., Characterization of the intrinsic and TSC2-GAP-regulated GTPase activity of Rheb by real-time NMR. *Sci Signal* **2009**, 2, (55), ra3.
2. Ritchie TK, G. Y., Bayburt TH, Denisov IG, Zolnerciks JK, Atkins WM, Sligar SG., Reconstitution of Membrane Proteins in Phospholipid Bilayer Nanodiscs. *Methods Enzymol* **2009**, 464, 211-231.
3. Kobashigawa, Y.; Harada, K.; Yoshida, N.; Ogura, K.; Inagaki, F., Phosphoinositide-incorporated lipid-protein nanodiscs: A tool for studying protein-lipid interactions. *Anal Biochem* **2011**, 410, (1), 77-83.
4. Goddard, T. D.; Kneller, D. *SPARKY 3*.
5. Farrow NA, Z. O., Szabo A, Torchia DA, Kay LE., Spectral density function mapping using 15N relaxation data exclusively. *J Biomol NMR.* **1995**, 6, (2), 153-162.
6. Marshall, C. B.; Meiri, D.; Smith, M. J.; Mazhab-Jafari, M. T.; Gasmi-Seabrook, G. M.; Rottapel, R.; Stambolic, V.; Ikura, M., Probing the GTPase cycle with real-time NMR: GAP and GEF activities in cell extracts. *Methods* **2012**, 57, (4), 473-85.
7. Chris Loken, D. G., Leslie Groer, Richard Peltier, Neil Bunn, Michael Craig, Teresa Henriques, Jillian Dempsey, Ching-Hsing Yu, Joseph Chen, L Jonathan Dursi, Jason Chong, Scott Northrup, Jaime Pinto, Neil Knecht and Ramses Van Zon, SciNet: Lessons Learned from Building a Power-efficient Top-20 System and Data Centre. *J. Phys.: Conf. Ser.* **2010**, 256, 012026.
8. de Vries, S. J.; van Dijk, A. D.; Krzeminski, M.; van Dijk, M.; Thureau, A.; Hsu, V.; Wassenaar, T.; Bonvin, A. M., HADDOCK versus HADDOCK: new features and performance of HADDOCK2.0 on the CAPRI targets. *Proteins* **2007**, 69, (4), 726-33.
9. Dominguez, C.; Boelens, R.; Bonvin, A. M., HADDOCK: a protein-protein docking approach based on biochemical or biophysical information. *J Am Chem Soc* **2003**, 125, (7), 1731-7.
10. Nederveen, A. J.; Doreleijers, J. F.; Vranken, W.; Miller, Z.; Spronk, C. A.; Nabuurs, S. B.; Guntert, P.; Livny, M.; Markley, J. L.; Nilges, M.; Ulrich, E. L.; Kaptein, R.; Bonvin, A. M., RECOORD: a recalculated coordinate database of 500+ proteins from the PDB using restraints from the BioMagResBank. *Proteins* **2005**, 59, (4), 662-72.
11. Yu, Y.; Li, S.; Xu, X.; Li, Y.; Guan, K.; Arnold, E.; Ding, J., Structural basis for the unique biological function of small GTPase RHEB. *J Biol Chem* **2005**, 280, (17), 17093-100.
12. Segrest, J. P.; Jones, M. K.; Klon, A. E.; Sheldahl, C. J.; Hellinger, M.; De Loof, H.; Harvey, S. C., A detailed molecular belt model for apolipoprotein A-I in discoidal high density lipoprotein. *J Biol Chem* **1999**, 274, (45), 31755-8.

13. Andrey Filippov, Greger Orädd, and Göran Lindblom, Influence of Cholesterol and Water Content on Phospholipid Lateral Diffusion in Bilayers. *Langmuir* **2003**, 19, (16), 6397–6400.
14. Otting, G., Protein NMR Using Paramagnetic Ions. *Annu. Rev. Biophys.* **2010**, 39, 387–405.
15. Kleywegt, G. J.; Henrick, K.; Dodson, E. J.; van Aalten, D. M., Pound-wise but penny-foolish: How well do micromolecules fare in macromolecular refinement? *Structure* **2003**, 11, (9), 1051-9.
16. Malde AK, Z. L., Breeze M, Stroet M, Poger D, Nair PC, Oostenbrink C, Mark AE., An Automated force field Topology Builder (ATB) and repository: version 1.0. *Journal of Chemical Theory and Computation* **2011**, 7, (12), 4026-4037.
17. Xavier Daura, K. G., Bernhard Jaun, Dieter Seebach, Wilfred F. van Gunsteren and Alan E. Mark, Peptide Folding: When Simulation Meets Experiment. *Angewandte Chemie International Edition* **1999**, 38, (1-2), 236-240.
18. Brunger, A. T.; Adams, P. D.; Clore, G. M.; DeLano, W. L.; Gros, P.; Grosse-Kunstleve, R. W.; Jiang, J. S.; Kuszewski, J.; Nilges, M.; Pannu, N. S.; Read, R. J.; Rice, L. M.; Simonson, T.; Warren, G. L., Crystallography & NMR system: A new software suite for macromolecular structure determination. *Acta Crystallogr D Biol Crystallogr* **1998**, 54, (Pt 5), 905-21.
19. Baker, N. A.; Sept, D.; Joseph, S.; Holst, M. J.; McCammon, J. A., Electrostatics of nanosystems: application to microtubules and the ribosome. *Proc Natl Acad Sci U S A* **2001,** 98, (18), 10037-41.